

First results with the `boloSource()` algorithm: Photometry of faint standard stars observed by Herschel/PACS

MARTON, G. · Vavrek, R. · Kiss, Cs. ·
Müller, Th. G.

Received: date / Accepted: date

Abstract The `boloSource()` algorithm is a tool to separate the signal of compact sources from that of the diffuse background in the timeline of far-infrared measurements performed by the PACS camera of the Herschel Space Observatory. An important characteristic and quality indicator of this method is that how well it can reproduce the flux of faint standard stars which have reliable flux estimates. For this propose we selected a few calibrator targets and constructed light curves by extracting point source flux for each repetition of the measurements independently using standard aperture photometry methods. These were compared with the light curves obtained using the `boloSource()` method on the same dataset. The results indicate that `boloSource()` provides a similar level of photometric accuracy and reproducibility as the usual flux extraction and photometry methods. This new technique will be developed further and also tested against other methods in more complex fields with the goal to make it usable for large-scale studies in the future.

Keywords PACS · timeline · photometry · faint sources

1 Introduction

The original goal of the development of the `boloSource()` algorithm (Vavrek et al., in prep.) is to create a tool which can provide source-free (i.e. background

G. Marton, Cs. Kiss
Konkoly Observatory, Research Center for Astronomy and Earth Sciences, Hungarian Academy of Sciences; Konkoly Thege 15-17, 1121 Budapest, Hungary
E-mail: marton.gabor@csfk.mta.hu

R. Vavrek
ESA/ESAC PO Box 50727 Villafranca del Castillo, 28080 Madrid, Spain

Th. G. Müller
Max-Planck-Institut für extraterrestrische Physik (MPE), Giessenbachstrasse, 85748, Garching, Germany

only) maps of the Herschel Space Observatory observations. This kind of maps are useful because analysis of the extended emission requires maps that are free of contaminating sources. Even in the Fourier space, compact objects (the extension of the source is around, or smaller than the beam FWHM at given wavelength) contribute to the image power spectra with a significant power at a broad range of spatial frequencies, and they modify the image at frequencies comparable to the beam-size. Depending on the surface density and the clustering strength, lower spatial frequencies are contaminated with a smaller power density but typically at large bandwidth. Detailed description of power spectra calculated from Herschel observations can be found in [4]. Image analysis techniques are difficult to compare if sources are not subtracted, because their sensitivity to discrete sub-structures may be quite different. Techniques using sparsity information could be falsified by even a few point sources, while techniques analyzing full intensity maps are more sensitive to clustering. For extended emission analysis we need a technique to subtract sources that fall within a well defined range of spatial frequencies and fulfill a major requirement: preserve noise properties of the image! The classical way to do that is to try to model the source intensity $I(x, y)$ in the Level 2 (L2, [3]) position-position space. But it is possible to reduce the problem to 1D in the Level 1 (L1, [3]) detector timeline. The sources can be subtracted from the detector timeline, followed by a re-projection of the source-free image.

2 Concept & method

2.1 Timeline interpolation

The detailed description of the algorithm is a subject of a future paper (Vavrek et al., in prep.). Here we present only a short outline of the concept. The timeline $I(t)$ has reduced dimensionality compared to the $I(x, y)$ position-position space, but the noise spectrum is more complex.

$$I(t) = N_{(t)}^{1/f} + N_{(t)}^D + N_{(t)}^{\text{det}} + I_{(t)}^S \quad (1)$$

In Eq. (1) $N_{(t)}^{1/f}$ stands for the $1/f$ noise, $N_{(t)}^D$ is the drift noise, $N_{(t)}^{\text{det}}$ is the detector noise and the source intensity is expressed by $I_{(t)}^S$. In the L1 timeline we also have a lower S/N than what we have in the L2 reconstructed maps. We are mainly interested in the subtraction of the high-frequency components. The L2 source masks are back-projected to the L1 timeline based on the celestial coordinates assigned to each L1 readout. The mask sizes are chosen to fully cover the apparent extent of a given source. We use stationary wavelet transform to decompose the signal, and to separate the low frequency baseline and the high frequency noise. This high frequency component is then used to Monte-Carlo simulate the noise on the masked section of the timeline. The algorithm applies a Monte-Carlo simulated (representative $1/f$) noise for the high-frequency part of the interpolated section. The reason behind is that the

timeline noise properties would be discontinued by a simple interpolation (e.g. applying a polynomial or a smooth baseline). Map reconstruction techniques may change their response in terms of introducing local artefacts (aka reconstruction noise) around the masked area, and change noise properties all over the image.

The size of the masked section is adaptive. The initial mask is first extended by a user-given factor and the determination of the final size is based on the first and last readouts which are below the estimated baseline. The interpolated signal on this section of the timeline is then produced as the sum of the low frequency baseline (sky background) and the Monte-Carlo simulated noise. An example of the timeline interpolation procedure is shown in Fig. 1. This technique also allows us to separate the source intensity from the extended emission and to create source-only and source-free maps at the same time.

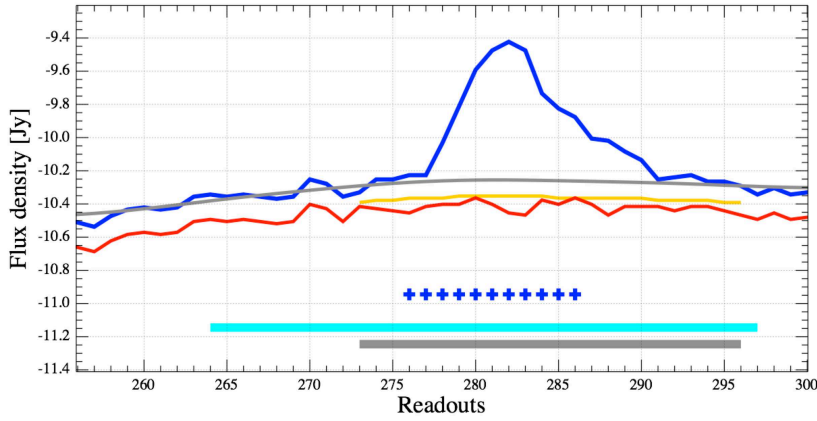


Fig. 1 A part of the L1 timeline with a contribution of a compact source in the middle. Blue solid line represent the original timeline. Gray solid line represent the estimated baseline (sky background), red and yellow lines represent the Monte-Carlo simulated and Gaussian noise shifted with -0.1 and -0.2 mJy for better visibility, respectively. Blue crosses, cyan and gray thick lines at the bottom of the figure represent the back-projected input mask defined by the user, the extended intermediate working mask and the optimized mask, respectively.

2.2 Comparison method

To find out if the algorithm is working properly, one needs to run various tests. As a first test, we subtracted standard stars with known brightness values from

the background, followed by the re-projection of the timeline that contains only the source flux. These sources were measured by the PACS instrument [8] in mini-scanmap mode [5], with $20''/s$ scan-speed. More information on the mini-scan-map mode and on the absolute flux calibration can be found in [1], while details about the general scan-map technique can be found in [9]. The reason of these observations was to test the PACS photometry on faint, but reliable stars. Their predicted brightness at the three nominal PACS wavelengths were calculated from photospheric models. The values are listed in Table 1. Note that the blue detector array observed either in the blue band ($70\mu\text{m}$) or in the green band ($100\mu\text{m}$), in the case of a specific OBSID, while the red data was always taken. It means that we have a mixed sample of blue and green band maps for the short wavelength detector array. As an example, we present an original, a source-free and a source-only map in Fig. 3.

In the first step the reliability of the standard star brightness was checked with the following method. Each observation consists of multiple repetitions. Starting from the first one, 2 consecutive repetitions were merged then high-pass filtering was used with high-pass filter width of 16, 18 and 36 readouts and were projected with the photProject task using pixel sizes of $1.1''$, $1.4''$ and $2.1''$ for the 70, 100 and $160\mu\text{m}$ observations, respectively. The observed flux was then calculated with the built-in aperture photometry pipeline of the HIPE [7] and also with the use of the IDL (Interactive Data Language) "aper" routine. While the HIPE task includes aperture correction, for the IDL photometry we used the encircled energy fraction (EEF) values listed in Table 15 of [6]. We also applied color correction assuming a black body temperature of 5000 K. For the flowchart of the regular photometry see the left column of Fig 2. From the measured points a light curve was constructed in each case and the standard deviation (σ) of the light curve points was calculated. In order to rule out the uncertainty of the instrument pointing, we constructed light curves with different aperture radius sizes ranging from $2''$ to $10''$, and checked if the photometric stability increases with aperture size. The average brightness of a given light curve was also calculated and was compared to the predicted one. The light curves are characterized by the standard deviation of the point source fluxes around the average (σ) and by the correction factor C which is the ratio of the average measured flux to the predicted flux ($C = \overline{F}_{\text{meas}}/F_{\text{pred}}$).

In the second step the source-only maps were created with the photProject task without the application of the high-pass filter method, with the same pixel sizes as given earlier. We determined the boloSource() flux values with the IDL "aper" routine and described the light curves in the same way as we did for the untouched maps. For the flowchart of the boloSource() photometry see the right column of Fig 2. For consistency and comparison we used the brightness values derived with IDL "aper" routine on both the original and source-only maps.

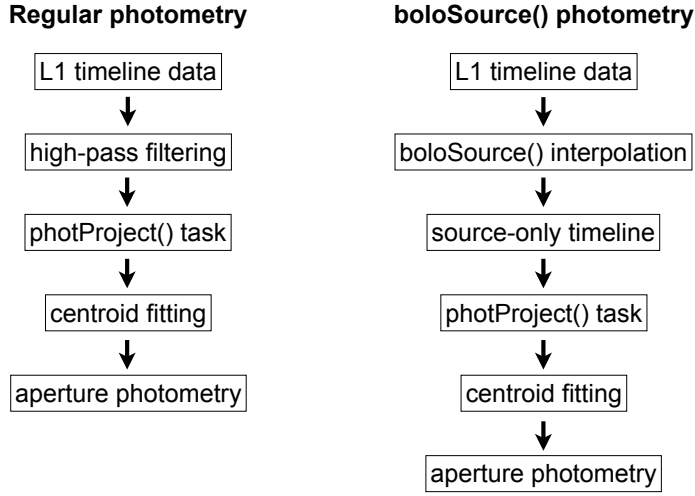


Fig. 2 Flowchart of the regular photometry produced on maps with nominal sky including background contamination (left chain) and the flowchart of the `boloSource()` photometry on the background-free maps (right chain). For details see text.

Table 1 Parameters of the standard stars used in testing the photometric capabilities of the `boloSource()` algorithm. Columns are as follows: source ID, spectral type and predicted brightness at 70, 100 and 160 μm with their corresponding uncertainty, respectively. Predicted flux values and their uncertainties at 70 μm are taken from [2]. Values for the 100 and 160 μm were calculated. Uncertainties for HD 139669 were not available.

Name	SpType	70 μm [mJy]	100 μm [mJy]	160 μm [mJy]
HD 15008	A1/2V	22.0 ± 0.8	10.8 ± 0.4	4.2 ± 0.2
HD 152222	K2III	37.9 ± 1.8	18.6 ± 0.9	7.3 ± 0.3
HD 39608	K5III	29.6 ± 1.2	14.6 ± 0.6	5.7 ± 0.2
HD 159330	K2III	61.7 ± 2.0	30.2 ± 1.0	11.8 ± 0.4
HD 139669	K5III	286	140	54
HD 138265	K5III	111.4 ± 3.8	54.6 ± 1.9	21.3 ± 0.7
HD 170693	K1.5III	147.7 ± 4.4	72.4 ± 2.2	28.3 ± 0.8

3 Results

As the example light curves show in Fig. 4, the brightness of the standard stars show some variation along the repetitions. This variation depends neither on the method used to derive the photometric values, nor on the size of the aperture radius. Therefore, we did not calculate all the brightness values with all aperture radii, but only with 5.0'', 6.0'' and 7.0'' at 70, 100 and 160 μm ,

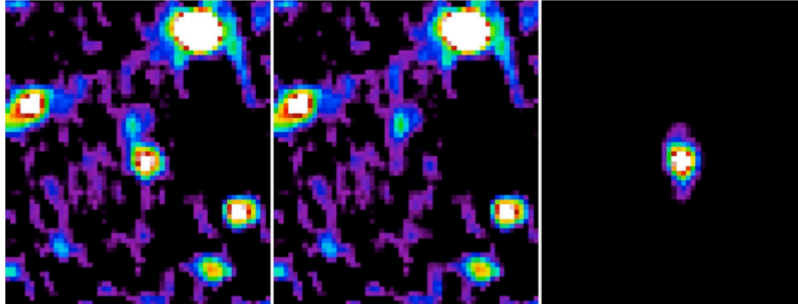


Fig. 3 Map of HD 170693 observed at $160\ \mu\text{m}$. The three panels are maps created using the original timeline (left), the interpolated timeline (middle) and the source-only timeline (right).

respectively. Comparison of the different methods were made in each band, individually.

- The results obtained at $70\ \mu\text{m}$ are listed in Table 2 and are plotted in Fig. 5. The median values of σ (the standard deviations of the point source flux) were found to be 2.02 mJy in the case of the original maps and 3.19 mJy in the case of the `boloSource()` case, while the averages were found to be 2.03 mJy and 2.89 mJy. The median of C correction factors are 0.99 and 1.01 in the original and `boloSource()` case, respectively, while the averages are 0.97 and 1.00.
- $100\ \mu\text{m}$ results are listed in Table 3 and are plotted in Fig. 6. For the original and for the `boloSource()` cases the median σ values were found to be 3.32 mJy and 3.80 mJy, while the average σ values were found to be 2.77 mJy and 3.65 mJy. The median C values are 1.04 and 1.06, while the average C values are 1.01 and 1.04.
- The $160\ \mu\text{m}$ results are listed in Table 4 and are plotted in Fig. 7. The median σ values from original and `boloSource()` cases are 6.50 mJy and 4.24 mJy, while the average σ values were found to be 6.54 mJy and 4.81 mJy. The median C values are 1.55 and 1.12, while the averages are 1.78 and 1.09.

4 Summary

In this work we demonstrated the use of the `boloSource()` on low and flat background. Point sources were subtracted and source-only maps were created from timeline data that contained only the source flux. Comparison of photometry on the source-only maps and on the original maps was made. This analysis is a first step in our testing of the `boloSource()` capabilities, and we were able to draw statistically reliable uncertainties. Such high repetition fac-

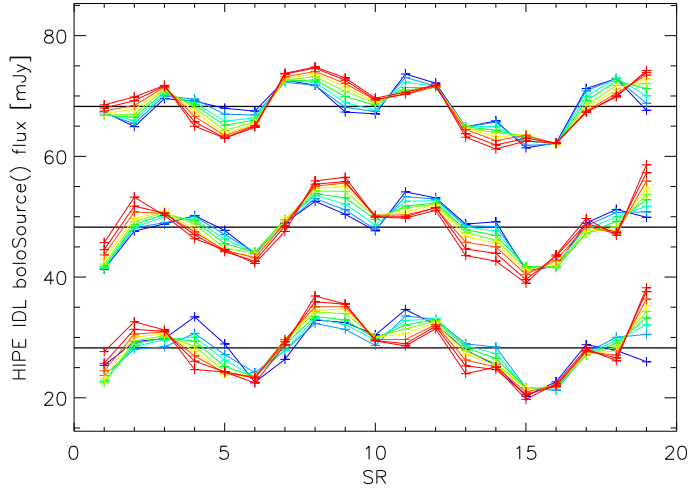


Fig. 4 HIPE (bottom), IDL (middle) and boloSource() (top) light curves of HD 170693 at $160\mu\text{m}$ as a function of repetition number. Colours from blue to red indicate the different aperture radii from $2''$ to $10''$. IDL and boloSource() values are shifted with $+20$ and $+40$ mJy for better visibility.

Table 2 σ and C parameters calculated for the standard star light curves at $70\mu\text{m}$. Columns are as follows: 1)Standard star name, 2)Observational ID of the Herschel observation from which the light curve was derived, 3)Number of repetitions in the measurement, 4)Predicted brightness of the star, 5)-6) σ and C values calculated for IDL brightness values, 7)-8) σ and C values calculated for boloSource() brightness values.

Name	OBSID	Repetitions	Brightness [mJy]	σ_{IDL}	C_{IDL}	$\sigma_{\text{bS}()}$	$C_{\text{bS}()}$
HD 15008	1342189130	9	22.0	3.63	1.05	3.58	1.00
HD 15008	1342189131	9	22.0	3.18	0.77	3.19	0.95
HD 152222	1342240702	6	37.9	3.71	0.98	5.31	1.01
HD 152222	1342240703	6	37.9	1.72	1.10	1.40	1.10
HD 152222	1342191964	6	37.9	1.06	0.97	1.23	0.96
HD 152222	1342191965	6	37.9	0.46	1.06	1.49	1.05
HD 39608	1342198535	10	29.7	2.10	1.08	3.75	1.10
HD 39608	1342198536	10	29.7	2.02	0.99	2.89	0.97
HD 159330	1342213585	6	61.7	1.40	1.00	0.35	1.01
HD 159330	1342213586	6	61.7	1.51	1.05	2.28	1.07
HD 139669	1342191982	6	286	0.93	0.84	4.01	0.87
HD 139669	1342191983	6	286	1.97	0.84	4.52	0.87
HD 138265	1342188841	21	111.4	2.31	0.90	2.94	0.98
HD 138265	1342188842	21	111.4	2.42	0.99	3.45	1.02

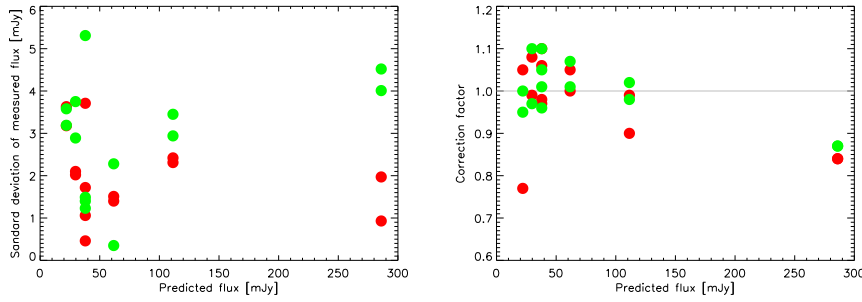


Fig. 5 σ (left panel) and C (right panel) values plotted as a function of the predicted brightness in the $70\mu\text{m}$ case. Red filled circles present the values calculated from the original maps, green symbols present the `bolosource()` values.

Table 3 Same as Table 2, for the $100\mu\text{m}$ case.

Name	OBSID	Repetitions	Brightness [mJy]	σ_{IDL}	C_{IDL}	$\sigma_{\text{bs}()}$	$C_{\text{bs}()}$
HD 152222	1342227973	33	18.6	2.42	1.04	3.59	1.09
HD 152222	1342227974	33	18.6	3.50	1.07	3.80	1.11
HD 159330	1342188839	10	30.2	4.74	1.02	5.30	1.05
HD 159330	1342188840	10	30.2	3.32	1.05	3.21	1.06
HD 138265	1342191986	6	54.6	1.81	0.94	1.53	0.98
HD 138265	1342191987	6	54.6	0.81	0.93	4.46	0.94

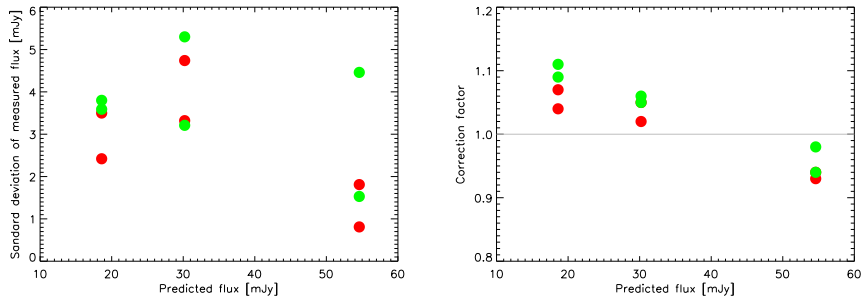


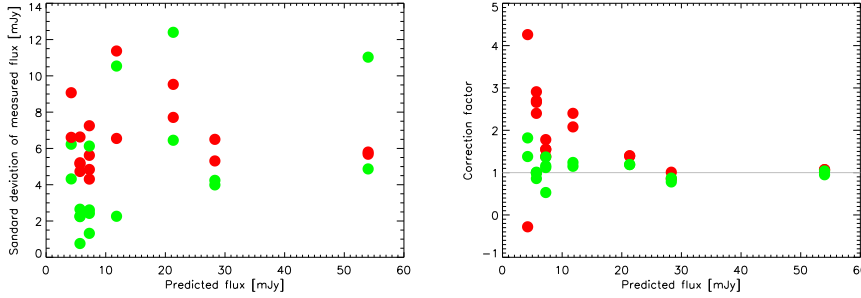
Fig. 6 Same as Fig. 5, for the $100\mu\text{m}$ case.

tor observations do not exist for crowded fields. Therefore, well isolated single point source measurements with multiple repetitions were used.

We conclude that on low and flat background the results of our method are fully comparable to the regular aperture photometry, the average and the median of σ values calculated with the two different methods agree well within ~ 1 mJy difference. Given the $\sim 5\%$ absolute flux accuracy of the measurements [6] and the uncertainty of the predicted brightness values, the comparison of the C correction factors show that `bolosource()` is also reliable in recovering the predicted absolute flux. From shorter to longer wavelengths the flux uncer-

Table 4 Same as Table 2, for the $160\mu\text{m}$ case.

Name	OBSID	Repetitions	Brightness [mJy]	σ_{IDL}	C_{IDL}	$\sigma_{\text{BS}()}$	$C_{\text{BS}()}$
HD 15008	1342189130	9	4.21	6.58	-0.05	7.78	1.07
HD 15008	1342189131	9	4.21	7.57	0.93	6.20	1.00
HD 152222	1342240702	6	7.25	0.05	0.90	2.21	0.67
HD 152222	1342240703	6	7.25	5.79	1.37	3.80	1.38
HD 152222	1342191964	6	7.25	3.98	1.26	1.58	1.30
HD 152222	1342191965	6	7.25	4.49	1.41	2.71	1.26
HD 39608	1342198535	10	5.68	4.21	1.87	0.82	1.28
HD 39608	1342198536	10	5.68	5.21	1.90	2.33	1.15
HD 39608	1342198537	35	5.68	6.66	1.61	2.32	1.18
HD 39608	1342198538	35	5.68	5.14	1.99	2.76	1.05
HD 159330	1342213585	6	11.81	3.17	1.26	1.97	1.09
HD 159330	1342213586	6	11.81	4.04	0.72	7.57	0.91
HD 139669	1342191982	6	54.0	5.31	1.01	7.72	1.00
HD 139669	1342191983	6	54.0	7.57	0.97	7.54	0.89
HD 138265	1342188841	21	21.32	8.22	0.83	9.93	1.11
HD 138265	1342188842	21	21.32	7.38	0.81	4.79	1.11
HD 170693	1342243730	20	28.3	6.50	0.85	3.99	0.78
HD 170693	1342243731	20	28.3	5.31	1.01	4.24	0.87

**Fig. 7** Same as Fig. 5, for the $160\mu\text{m}$ case.

tainty is decreased using our method compared with the regular photometry, while the accuracy of the recovered flux is increased.

We note that `boloSource()` is still under development with the goal of making it usable for large-scale studies. The test environment need to be extended to simulated data sets that can mimic the low-redundancy complex galactic fields. We plan to add simulated point sources in a wide flux range to a simulated cirrus background. Test cases will cover various positions on the surface-brightness vs. background complexity parameter space. We expect that `boloSource()` provides an increasing efficiency towards the more complex cases (better than aperture photometry) but this statement is to be justified. Our goals also include an extension to the SPIRE photometer observations. Detailed description of the algorithm, and the further tests and results are subject of a future paper.

Acknowledgements We thank our anonymous referee whose comments significantly improved the manuscript. We thank Z. Balog for the useful discussion. This work has been supported by the following grants: i) PECS contract no. 98073 of the Hungarian Space Office and the European Space Agency, ii) Hungarian Research Fund (OTKA) grants nr. 101939 and 104607. C.K. acknowledges the support of the Bolyai Research Fellowship of the Hungarian Academy of Sciences. We acknowledge support from the Faculty of the European Space Astronomy Centre (ESAC).

References

1. Balog, Z., Müller, T. G., Nielbock, M. et al., The Herschel-PACS photometer calibration: Point-source flux calibration, *Exp. Astronomy*, this issue (2013)
2. Gordon, K. D., Engelbracht, C. W., Fadda, D. et al., Absolute Calibration and Characterization of the Multiband Imaging Photometer for Spitzer. II. 70 μm Imaging, *PASP*, 119, 1019 (2007)
3. Herschel Science Centre, Herschel Observers' Manual, HERSCHEL-HSC-DOC-0876, version 4.1.4 (2013)
4. Martin, P. G., Miville-Deschênes, M.-A., Roy, A. et al., Direct estimate of cirrus noise in Herschel Hi-GAL images, *A&A*, 518, 105 (2010)
5. Müller, T. G., PACS Photometer - Point/Compact Source Observations: Mini Scan-Maps & Chop-Nod, PACC-ME-TN-036
6. Müller, T. G., Nielbock, M., Balog, Z., Klaas, U., Vilenius, E., PACS Photometer - Point-Source Flux Calibration, PACC-ME-TN-037, PACS ICC Release Note (2011)
7. Ott, S., The Herschel Data Processing System HIPE and Pipelines Up and Running Since the Start of the Mission, *ASPC*, 434, 139 (2010)
8. Poglitsch, A., Waelkens, C., Geis, N. et al., The Photodetector Array Camera and Spectrometer (PACS) on the Herschel Space Observatory, *A&A*, 518, 2 (2010)
9. The PACS ICC, PACS photometer - Prime and Parallel scan mode release note, PACC-ME-TN-035, PACS ICC Release Note (2010)